Acta Mech 223, 861–878 (2012)
DOI 10.1007/s00707-011-0607-7

Chris B. Kandilas

Transient elastodynamic analysis of nonhomogeneous anisotropic plane bodies

Received: 1 August 2011 / Revised: 13 December 2011 / Published online: 17 January 2012

Abstract A boundary-only BEM procedure is employed to solve the transient dynamic analysis of nonhomogeneous anisotropic plane elastic bodies. The response of such bodies is governed by two coupled linear, second-order hyperbolic PDEs with spatially dependent coefficients. The lack of a reliable 2D time-domain elastodynamic fundamental solution is overcome using the principle of the Analog Equation, a method by which the equations of motion of the problem are substituted by two coupled quasi-static Poisson-type equations having as nonhomogeneous terms the components of a fictitious time-dependent load distribution in the specified domain. The standard BEM is employed for the solution of the substitute equations. To avoid the appearance of the domain integral in the integral representation of the solution, the fictitious load distribution is approximated by multiquadrics with unknown time-dependent expansion coefficients, which are calculated at discrete timepoints by collocating the equations of motion at a predefined set of domain interpolation nodes. The obtained numerical results by the proposed method demonstrate its stability and accuracy over other numerical methods.

1 Introduction

The current paper presents a BEM-based solution for the transient dynamic analysis of 2D nonhomogeneous anisotropic elastic solids. Engineering applications using materials such as the functionally graded materials were developed over the past years, since they offered attractive properties of strength and stiffness. This continuously increasing field of applications requires accurate computational methods for the calculation of stress and strain fields. The inhomogeneity and anisotropy of such plane bodies result from the position and directional dependence of the material elastic parameters. Their response is described by an initial-boundary value problem involving second-order partial differential equations of hyperbolic type with spatially dependent coefficients. Due to the importance of obtaining a solution for such problems, several techniques have been developed. With regard to boundary integral equation methods, though extended literature is available for the dynamic problem of isotropic bodies [1], few works are found for analyzing dynamic anisotropic problems [2,3]. The reason is that the conventional BEM exhibits a major drawback for this type of problems due to the absence of well-established fundamental solutions. Most anisotropic fundamental solutions for elastodynamics require numerical integration [4,5]. An alternative approach is the application of static fundamental solutions by considering inertia terms as body forces. In this case, the most suitable fundamental solutions are those proposed by Cruse and Swedlow [6], which require no numerical integration. The fact that domain integrals appear in the boundary element formulation due to inertia terms is worth noting. These domain integrals can be transformed into boundary integrals using appropriate techniques. Albuquerque et al. [7,8] used the dual

C. B. Kandilas (✉)
Division of Applied Mechanics and Marine Materials, Hellenic Naval Academy, Piraeus, Greece
E-mail: chkan@snd.edu.gr
Tel.: +030-210-9651729
Fax: +030-210-9651729

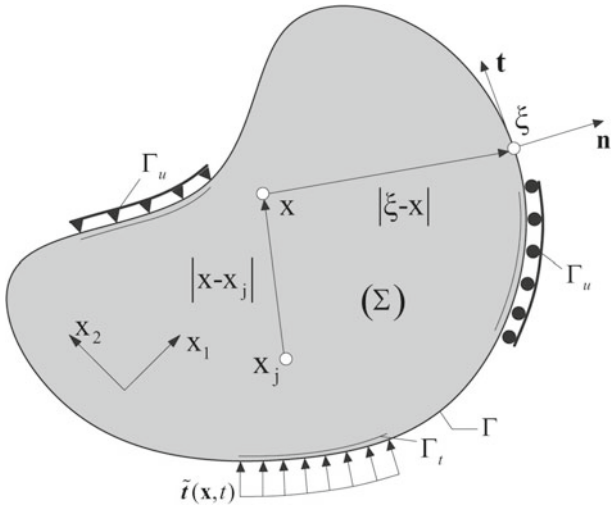

Fig. 1 Domain occupied by the body and notation

reciprocity BEM (DR/BEM) to solve problems of anisotropic media. During the last years, more advanced methods have been developed for the solution of initial-boundary value problems on complex domains. These so called meshless methods based on local weak-form formulations on global or on a set of local subdomains were successfully applied to isotropic homogeneous and continuously inhomogeneous bodies under static (Atluri et al. [9]; Sladek et al. [10,11]) and dynamic loads (Sladek et al. [12]). Also, Sladek et al. [13,14] presented a meshless method based on the local Petrov–Galerkin approach for the solution of static and elastodynamics problems in a homogeneous anisotropic medium. In the presented new formulation, a domain meshless boundary element technique is introduced for the dynamic analysis of this particular type of problems using the principle of the Analog Equation Method [15–19]. The method substitutes the equations of motion by two equivalent quasi-static Poisson-type equations with fictitious domain loads, under the same boundary and initial conditions. The introduced unknown field load functions are approximated by a radial basis functions series (RBF) of multiquadric type in which the time-dependent expansion coefficients are evaluated by collocating the problem equations [20]. The procedure results in a discretized form of equations in terms of the expansion coefficients, on a selected number of collocation points which are solved in the time domain of interest using a direct time integration scheme. The presented method maintains the pure boundary character of the BEM, since the discretization into elements and the integrations are limited only to the boundary of the domain. Several example problems are studied to demonstrate the accuracy of the method.

2 Governing equations and problem statement

We consider a nonhomogeneous, anisotropic, linear elastic body with mass density distribution $\rho(\mathbf{x})$, occupying a bounded region $\Sigma \subseteq \mathbb{R}^3$ (Fig. 1). The boundary Γ of Σ is divided into the part $\Gamma_u \subseteq \Gamma$, where the displacement vector $\tilde{\boldsymbol{u}}(\mathbf{x}, t)$ is specified and into $\Gamma_t (= \Gamma - \Gamma_u)$, where the boundary traction vector $\tilde{\boldsymbol{t}}(\mathbf{x}, t)$ is specified. Furthermore, the body may be subjected to a distribution of time-dependent body forces $\boldsymbol{b}(\mathbf{x}, t)$. Referred to a selected Cartesian frame $O\mathrm{x}_1\mathrm{x}_2\mathrm{x}_3$, the dynamic response of the body within the time domain of interest $[0, T]$ is governed by the following differential equations of linearized elastodynamics:

$$\sigma_{ij,j}(\mathbf{x}, t) + b_i(\mathbf{x}, t) = \rho(\mathbf{x})\ddot{u}_i(\mathbf{x}, t) \quad \text{in} \quad \Sigma \times [0, T], \tag{1}$$

with boundary conditions

$$u_i(\mathbf{x}, t) = \tilde{u}_i(\mathbf{x}, t) \quad \text{on} \quad \Gamma_u \times [0, T], \tag{2.1}$$

$$\sigma_{ij}(\mathbf{x}, t)n_j(\mathbf{x}) = \tilde{t}_i(\mathbf{x}, t) \quad \text{on} \quad \Gamma_t \times [0, T], \tag{2.2}$$

and initial conditions

$$u_i(\mathbf{x}, 0) = \tilde{u}_i(\mathbf{x}, 0), \tag{3.1}$$

$$\dot{u}_i(\mathbf{x}, 0) = \dot{\tilde{u}}_i(\mathbf{x}, 0), \tag{3.2}$$

where $\boldsymbol{n}(\mathbf{x}) = (n_1, n_2)$ is the unit vector along the outer normal to the boundary at $\mathbf{x}$, $\sigma_{ij} = \sigma_{ij}(\mathbf{x}, t)$ are the components of the Cauchy stress tensor with respect to the selected coordinate system determined in terms of displacements by the generalized Hooke's law,

$$\sigma_{ij}(\mathbf{x}, t) = C_{ijkl}(\mathbf{x}) u_{k,l}(\mathbf{x}, t), \tag{4}$$

where summation over repeated indices is implied; $C_{ijkl}(\mathbf{x})$ are the components of the fourth-order elasticity modulus tensor $\mathbf{C}$, which are assumed to satisfy the major and minor conditions for symmetry. Throughout this work, the superposed dot over a quantity indicates partial differentiation with respect to time, and the comma denotes differentiation with respect to spatial variables.

The tractions $t_i(\mathbf{x}, t)$ are related to displacements by Cauchy's formula for the strain,

$$t_i(\mathbf{x}, t) = C_{ijkl}(\mathbf{x}) u_{k,l}(\mathbf{x}, t) n_j(\mathbf{x}). \tag{5}$$

On substituting Eqs. (4) into (1) and carrying out the differentiations, the following field equations of motion in terms of displacements are obtained:

$$C_{ijkl,j}(\mathbf{x}) u_{k,l}(\mathbf{x}, t) + C_{ijkl}(\mathbf{x}) u_{k,jl}(\mathbf{x}, t) + b_i(\mathbf{x}, t) = \rho(\mathbf{x}) \ddot{u}_i(\mathbf{x}, t). \tag{6}$$

The most general anisotropic elastic solid requires for its description 21 elastic constants. However, for 2D cases, the number of independent constants is reduced to six. In this case, the indices of the components for $\mathbf{C}$ are simplified, and Eqs. (6) can be written in the following contracted form:

$$\mathcal{L}_{11}(u_1) + \mathcal{L}_{12}(u_2) + b_1 = \rho \ddot{u}_1, \tag{7.1}$$
$$\mathcal{L}_{21}(u_1) + \mathcal{L}_{22}(u_2) + b_2 = \rho \ddot{u}_2. \tag{7.2}$$

Moreover, if the spatial derivatives in Eqs. (2.1) are replaced in terms of the derivatives in the normal and tangential direction along the boundary, the following relations are valid:

$$\mathcal{T}_{11}(u_1) + \mathcal{T}_{12}(u_2) = \tilde{t}_1(\mathbf{x}, t), \tag{8.1}$$
$$\mathcal{T}_{21}(u_1) + \mathcal{T}_{22}(u_2) = \tilde{t}_2(\mathbf{x}, t). \tag{8.2}$$

The linear differential operators $\mathcal{L}_{ij}$ and $\mathcal{T}_{ij} (i, j = 1, 2)$ involved in Eqs. (7.1) and (8.1) are given by the expressions

$$\begin{aligned}\mathcal{L}_{11}(\cdot) = {} & c_{11}(\cdot)_{,11} + c_{16}(\cdot)_{,12} + c_{11,1}(\cdot)_{,1} + c_{16,1}(\cdot)_{,2} + c_{16}(\cdot)_{,12} \\ & + c_{66}(\cdot)_{,22} + c_{16,2}(\cdot)_{,1} + c_{66,2}(\cdot)_{,2},\end{aligned} \tag{9.1}$$
$$\begin{aligned}\mathcal{L}_{12}(\cdot) = {} & c_{16}(\cdot)_{,11} + c_{12}(\cdot)_{,12} + c_{16,1}(\cdot)_{,1} + c_{12,1}(\cdot)_{,2} + c_{66}(\cdot)_{,12} \\ & + c_{26}(\cdot)_{,22} + c_{66,2}(\cdot)_{,1} + c_{26,2}(\cdot)_{,2},\end{aligned} \tag{9.2}$$
$$\begin{aligned}\mathcal{L}_{21}(\cdot) = {} & c_{16}(\cdot)_{,11} + c_{12}(\cdot)_{,12} + c_{16,1}(\cdot)_{,1} + c_{12,2}(\cdot)_{,1} + c_{66}(\cdot)_{,12} \\ & + c_{26}(\cdot)_{,22} + c_{66,1}(\cdot)_{,2} + c_{26,2}(\cdot)_{,2},\end{aligned} \tag{9.3}$$
$$\begin{aligned}\mathcal{L}_{22}(\cdot) = {} & c_{66}(\cdot)_{,11} + c_{26}(\cdot)_{,12} + c_{66,1}(\cdot)_{,1} + c_{26,1}(\cdot)_{,2} + c_{26}(\cdot)_{,12} \\ & + c_{22}(\cdot)_{,22} + c_{26,2}(\cdot)_{,1} + c_{22,2}(\cdot)_{,2}\end{aligned} \tag{9.4}$$

and

$$\begin{aligned}\mathcal{T}_{11}(\cdot) = {} & [c_{16}(n_1^2 - n_2^2) + (c_{66} - c_{11}) n_1 n_2](\cdot)_{,s} + [c_{11} n_1^2 + c_{66} n_2^2 \\ & + 2 c_{16} n_1 n_2](\cdot)_{,n},\end{aligned} \tag{10.1}$$
$$\begin{aligned}\mathcal{T}_{12}(\cdot) = {} & [c_{12} n_1^2 + (c_{26} - c_{16}) n_1 n_2 - c_{66} n_2^2](\cdot)_{,s} + [(c_{12} + c_{66}) n_1 n_2 \\ & + c_{16} n_1^2 + c_{26} n_2^2](\cdot)_{,n},\end{aligned} \tag{10.2}$$
$$\begin{aligned}\mathcal{T}_{21}(\cdot) = {} & [-c_{12} n_2^2 + (c_{26} - c_{16}) n_1 n_2 + c_{66} n_1^2](\cdot)_{,s} + [(c_{12} + c_{66}) n_1 n_2 \\ & + c_{16} n_1^2 + c_{26} n_2^2](\cdot)_{,n},\end{aligned} \tag{10.3}$$
$$\begin{aligned}\mathcal{T}_{22}(\cdot) = {} & [c_{26}(n_1^2 - n_2^2) + (c_{22} - c_{66}) n_1 n_2](\cdot)_{,s} + [c_{66} n_1^2 + 2 c_{26} n_1 n_2 \\ & + c_{22} n_2^2](\cdot)_{,n}\end{aligned} \tag{10.4}$$

where $(.)_{,s}$ and $(.)_{,n}$ denote differentiation with respect to the arc length s of the boundary and the outward normal n to it, respectively.

For orthotropic materials, the number of independent material constants is reduced to four, and the related differential operators are extracted from expressions (9.1) and (10.1), setting $c_{16} = c_{26} = 0$. Equations (7.1) in the domain and (2.1), (8.1) on the boundary together with the initial conditions given by (3.1) formulate in terms of displacements a well-posed, second-order initial-boundary value problem for the spatially dependent hyperbolic equations of motion.

3 The AEM for the transient dynamic analysis of anisotropic 2D problems

The initial-boundary value problem, as stated above, is solved by implementing a boundary-only method based on the concept of Analog Equation [15–19], which is explained as follows.

Let $u_i(\mathbf{x}, t)$, $(i = 1, 2)$ be the components of the sought solution $\boldsymbol{u}(\mathbf{x})$ of the problem, twice continuously differentiable in $\Sigma \times [0, T]$ and once on the boundary $\Gamma \times [0, T]$. If we apply the 2D Laplacian operator on u_i, the following quasi-static Poisson-type equations:

$$\nabla^2 u_i(\mathbf{x}, t) = q_i(\mathbf{x}, t), \tag{11}$$

with unknown in the first instance fictitious time-dependent domain source densities are constructed.

The method suggests that the solution to the original problem could be obtained from the solution of the substitute Eq. (11) under the same boundary and initial conditions, if the source densities are properly calculated.

The transformation of Eq. (11), which will be called the analog equations, into integral equations is accomplished by employing the method of weighted residuals using as weighting function the well-known fundamental solution of the substitute equations. After employing Green's second identity, the displacements at $\mathbf{x} \in \Sigma \cup \Gamma$ are given by the following integral equation:

$$\varepsilon u_i(\mathbf{x}, t) = \int_{\Sigma} u^*(\mathbf{x}, \mathbf{y}) q_i(\mathbf{y}, t) d\Sigma_y - \int_{\Gamma} [u^*(\mathbf{x}, \boldsymbol{\xi}) u_{i,n}(\boldsymbol{\xi}, t) - u_i(\boldsymbol{\xi}, t) u^*_{,n}(\mathbf{x}, \boldsymbol{\xi})] \mathrm{d}\Gamma_{\xi}, \tag{12}$$

where $\mathbf{y} \in \Sigma$ and $\boldsymbol{\xi} \in \Gamma$; $u^*(\mathbf{x}, \mathbf{y}) = \ln r(\mathbf{x}, \mathbf{y})/2\pi$ is the fundamental solution of the Laplace equation and $u^*_{,n}(\mathbf{x}, \boldsymbol{\xi})$ its derivative in the normal direction to the boundary at $\boldsymbol{\xi}$; ε is a constant ($\varepsilon = 1$ for $\mathbf{x} \in \Sigma, \epsilon = \beta/2\pi$ for $\mathbf{x} \in \Gamma$, with β the internal angle between the tangents of the boundary at $\mathbf{x}$).

The approximation of the domain integral in (12) requires a predefined domain discretization into a number of internal cells. Even though this integral treatment has been shown to produce accurate results, it reduces the attraction of the BEM method over the domain-based numerical methods. In order to preserve the pure boundary character of the method, the fictitious source density functions are represented as a linear interpolation on a predefined pattern of nodes in the domain using the finite series representation

$$q_i(\mathbf{x}, t) = \sum_{j=1}^{M} \alpha_j^{(i)}(t) f_j(\mathbf{x}, \mathbf{x}_j), \tag{13}$$

where $f_j(\mathbf{x}, \mathbf{x}_j)$ belongs to a selected set $\{f_j\}_{j=1}^{M}$ of radial basis interpolation functions, and $\alpha_j^{(i)}(t)$ is the unknown expansion coefficient for the RBF f_j at the x_i direction, corresponding to the given point $\mathbf{x}_j$.

At any time t, the solution of the analog equations can be represented as the superposition of the homogeneous solution, $\bar{u}_i(\mathbf{x}, t)$, and a particular one, $u_i^p(\mathbf{x}, t)$. The latter can be approximated from a set of particular solutions $\{\hat{u}_j\}_{j=1}^{M}$ to the equations

$$\nabla^2 \hat{u}_j(\mathbf{x}) = f_j(\mathbf{x}, \mathbf{x}_j), \tag{14}$$

according to the following scheme:

$$u_i^p(\mathbf{x}, t) = \sum_{j=1}^{M} \alpha_j^{(i)}(t) \hat{u}_j(\mathbf{x}), \tag{15}$$

where $\hat{u}_j$ can always be determined by analytical integration when the RBFs $f_j(\mathbf{x}, \mathbf{x}_j)$ are selected.

On the other hand, the homogenous solution $\bar{u}_i(\mathbf{x}, t)$ can be approximated in terms of the expansion coefficients of the interpolation from the solution of the following boundary value problem:

$$\nabla^2 \bar{u}_i(\mathbf{x}, t) = 0 \quad \text{in} \quad \Sigma \times [0, T] \tag{16}$$

with

$$\bar{u}_i(\mathbf{x}, t) = \tilde{u}_i(\mathbf{x}, t) - \sum_{j=1}^{M} \alpha_j^{(i)}(t)\hat{u}_j(\mathbf{x}) \tag{17}$$

for $\mathbf{x} \in \Gamma_u \times [0, T]$ and

$$\mathcal{T}_{11}(\bar{u}_1) + \mathcal{T}_{12}(\bar{u}_2) = \tilde{t}_1(\mathbf{x}, t) - \sum_{j=1}^{M} \left[\alpha_j^{(1)}(t)\mathcal{T}_{11}(\hat{u}_j) + \alpha_j^{(2)}(t)\mathcal{T}_{12}(\hat{u}_j)\right], \tag{18.1}$$

$$\mathcal{T}_{21}(\bar{u}_1) + \mathcal{T}_{22}(\bar{u}_2) = \tilde{t}_2(\mathbf{x}, t) - \sum_{j=1}^{M} \left[\alpha_j^{(1)}(t)\mathcal{T}_{21}(\hat{u}_j) + \alpha_j^{(2)}(t)\mathcal{T}_{22}(\hat{u}_j)\right] \tag{18.2}$$

for $\mathbf{x} \in \Gamma_t \times [0, T]$.

Therefore, the solution $\bar{u}_i(\mathbf{x}, t)$ to the homogeneous Eq. (16) can be written in an integral form as

$$\varepsilon \bar{u}_i(\mathbf{x}, t) = \int_{\Gamma} [\bar{u}_i(\boldsymbol{\xi}, t)u,_n^*(\mathbf{x}, \boldsymbol{\xi}) - u^*(\mathbf{x}, \boldsymbol{\xi})\bar{u}_{i,n}(\boldsymbol{\xi}, t)]\mathrm{d}\Gamma_\xi. \tag{19}$$

On the basis of Eqs. (15) and (19), the solution to Eq. (11) for points $\mathbf{x} \in \Sigma$, setting $\varepsilon = 1$, is given by

$$u_i(\mathbf{x}, t) = \sum_{j=1}^{M} \alpha_j^{(i)}(t)\hat{u}_j(\mathbf{x}) + \int_{\Gamma} [\bar{u}_i(\boldsymbol{\xi}, t)u,_n^*(\mathbf{x}, \boldsymbol{\xi}) - u^*(\mathbf{x}, \boldsymbol{\xi})\bar{u}_{i,n}(\boldsymbol{\xi}, t)]\mathrm{d}\Gamma_\xi \tag{20}$$

and for points on the boundary by

$$\frac{\beta}{2\pi} u_i(\mathbf{x}, t) = \sum_{j=1}^{M} \alpha_j^{(i)}(t)\hat{u}_j(\mathbf{x}) + \int_{\Gamma} [\bar{u}_i(\boldsymbol{\xi}, t)u,_n^*(\mathbf{x}, \boldsymbol{\xi}) - u^*(\mathbf{x}, \boldsymbol{\xi})\bar{u}_{i,n}(\boldsymbol{\xi}, t)]\mathrm{d}\Gamma_\xi. \tag{21}$$

The spatial and time derivatives of the displacements are obtained from Eq. (20) dy direct differentiation, namely,

$$u_{i,pq}(\mathbf{x}, t) = \sum_{j=1}^{M} \alpha_j^{(i)}(t)\hat{u}_{j,pq}(\mathbf{x}) + \int_{\Gamma} [\bar{u}_i(\boldsymbol{\xi}, t)u,_{npq}^*(\mathbf{x}, \boldsymbol{\xi}) - u,_{pq}^*(\mathbf{x}, \boldsymbol{\xi})\bar{u}_{i,n}(\boldsymbol{\xi}, t)]\mathrm{d}\Gamma_\xi, \tag{22}$$

$$\dot{u}_i(\mathbf{x}, t) = \sum_{j=1}^{M} \dot{\alpha}_j^{(i)}(t)\hat{u}_j(\mathbf{x}) + \int_{\Gamma} [\dot{\bar{u}}_i(\boldsymbol{\xi}, t)u,_n^*(\mathbf{x}, \boldsymbol{\xi}) - u^*(\mathbf{x}, \boldsymbol{\xi})\dot{\bar{u}}_{i,n}(\boldsymbol{\xi}, t)]\mathrm{d}\Gamma_\xi, \tag{23}$$

$$\ddot{u}_i(\mathbf{x}, t) = \sum_{j=1}^{M} \ddot{\alpha}_j^{(i)}(t)\hat{u}_j(\mathbf{x}) + \int_{\Gamma} [\ddot{\bar{u}}_i(\boldsymbol{\xi}, t)u,_n^*(\mathbf{x}, \boldsymbol{\xi}) - u^*(\mathbf{x}, \boldsymbol{\xi})\ddot{\bar{u}}_{i,n}(\boldsymbol{\xi}, t)]\mathrm{d}\Gamma_\xi. \tag{24}$$

Application of the differential operators $\mathcal{L}_{pq}(p, q = 1, 2)$ on Eq. (20) leads to

$$\mathcal{L}_{pq}(u_i) = \sum_{j=1}^{M} \alpha_j^{(i)}\mathcal{L}_{pq}(\hat{u}_j) + \int_{\Gamma} [\bar{u}_i\mathcal{L}_{pq}(u,_n^*) - \mathcal{L}_{pq}(u^*)\bar{u}_{i,n}]\mathrm{d}\Gamma. \tag{25}$$

The next step of the method is the satisfaction of Eqs. (7.1) at the M collocation points inside Σ. Therefore, at each collocation point m, the equations of motion after substituting Eq. (25) become

$$\begin{aligned}
&\sum_{j=1}^{M}\left[\alpha_j^{(1)}\mathcal{L}_{11}^{(m)}(\hat{u}_j)+\alpha_j^{(2)}\mathcal{L}_{12}^{(m)}(\hat{u}_j)\right]+\int_{\Gamma}\left[\bar{u}_1\mathcal{L}_{11}^{(m)}(u,_n^*)+\bar{u}_2\mathcal{L}_{12}^{(m)}(u,_n^*)\right]\mathrm{d}\Gamma\\
&\quad-\int_{\Gamma}\left[\bar{u}_{1,n}\mathcal{L}_{11}^{(m)}(u^*)+\bar{u}_{2,n}\mathcal{L}_{12}^{(m)}(u^*)\right]\mathrm{d}\Gamma+b_1^{(m)}\\
&\quad=\rho\left\{\sum_{j=1}^{M}\ddot{\alpha}_j^{(1)}\hat{u}_j^{(m)}+\int_{\Gamma}\left[\ddot{\bar{u}}_1(u,_n^*)^{(m)}-\ddot{\bar{u}}_{1,n}(u^*)^{(m)}\right]\mathrm{d}\Gamma\right\},
\end{aligned}\tag{26.1}$$

$$\begin{aligned}
&\sum_{j=1}^{M}\left[\alpha_j^{(1)}\mathcal{L}_{21}^{(m)}(\hat{u}_j)+\alpha_j^{(2)}\mathcal{L}_{22}^{(m)}(\hat{u}_j)\right]+\int_{\Gamma}\left[\bar{u}_1\mathcal{L}_{21}^{(m)}(u,_n^*)+\bar{u}_2\mathcal{L}_{22}^{(m)}(u,_n^*)\right]\mathrm{d}\Gamma\\
&\quad-\int_{\Gamma}\left[\bar{u}_{1,n}\mathcal{L}_{21}^{(m)}(u^*)+\bar{u}_{2,n}\mathcal{L}_{22}^{(m)}(u^*)\right]\mathrm{d}\Gamma+b_2^{(m)}\\
&\quad=\rho\left\{\sum_{j=1}^{M}\ddot{\alpha}_j^{(2)}\hat{u}_j^{(m)}+\int_{\Gamma}\left[\ddot{\bar{u}}_2(u,_n^*)^{(m)}-\ddot{\bar{u}}_{2,n}(u^*)^{(m)}\right]\mathrm{d}\Gamma\right\}.
\end{aligned}\tag{26.2}$$

The boundary quantities $\bar{u}_i$, $\bar{u}_{i,n}$ can be eliminated from Eqs. (26.1) using a set of discretized relations obtained by collocating the BIE (21) and the boundary conditions (17) and (18.1) at a selected number of boundary nodes, using the standard BEM. In addition, numerical differentiation is employed to approximate $\bar{u}_{i,s}$ in terms of the boundary nodal values $\bar{u}_i$. After the elimination, the following $2M$ discretized system of equations in terms of the unknown expansion coefficients

$$\mathcal{F}_1^{(m)}(\alpha_j^{(1)},\alpha_j^{(2)},\ddot{\alpha}_j^{(1)})+b_1^{(m)}=0,\tag{27.1}$$

$$\mathcal{F}_2^{(m)}(\alpha_j^{(1)},\alpha_j^{(2)},\ddot{\alpha}_j^{(2)})+b_2^{(m)}=0\tag{27.2}$$

is formulated, which is solved numerically using an implicit time integration method preserving the initial conditions of the original problem. In this work, the approximating radial basis functions $f_j(\mathbf{x},\mathbf{x}_j)$ are selected to be the multiquadrics [20] defined from

$$f_j(\mathbf{x},\mathbf{x}_j)=\sqrt{r^2+c^2}\tag{28}$$

where $r=r(\mathbf{x},\mathbf{x}_j)$ is the Euclidean distance between the source $\mathbf{x}$ and the field point $\mathbf{x}_j$ and c an arbitrary constant defined as the shape parameter. In this work, an empirical-based selection of the shape parameter is avoided and the accuracy of the approximation is considerably improved by minimizing the potential that yields the domain equations of the static problem. Moreover, the number and the distribution of the collocation points are selected to best capture the nonhomogeneity and anisotropy of the material. Using the proposed f_j, the expressions of the particular solutions $\hat{u}_j$ are given by

$$\hat{u}_j=-\frac{c^3}{3}\left[\ln(2c^2)-\frac{4}{3}\right]\quad\text{for}\quad r=0,\tag{29.1}$$

$$\hat{u}_j=-\frac{c^3}{3}\left(c\sqrt{r^2+c^2}+c^2\right)+\frac{1}{9}(r^2+4c^2)\sqrt{r^2+c^2}\quad\text{for}\quad r\neq 0,\tag{29.2}$$

and the first and second derivatives with respect to x_i from

$$\hat{u}_{j,k} = \frac{1}{3\sqrt{r^2+c^2}}\left[r^2+2c^2-\frac{c^3}{\sqrt{r^2+c^2}+c}\right][x_k-(x_k)_j], \tag{30.1}$$

$$\hat{u}_{j,kk} = \frac{1}{3(r^2+c^2)^{3/2}}\left[r^2+c^3\frac{2\sqrt{r^2+c^2}+c}{\left(\sqrt{r^2+c^2}+c\right)^2}\right][x_k-(x_k)_j] + \frac{1}{3\sqrt{r^2+c^2}}\left[r^2+2c^2-\frac{c^3}{\sqrt{r^2+c^2}+c}\right], \tag{30.2}$$

$$\hat{u}_{j,kl} = \frac{1}{3(r^2+c^2)^{3/2}}\left[r^2+c^3\frac{2\sqrt{r^2+c^2}+c}{\left(\sqrt{r^2+c^2}+c\right)^2}\right][x_k-(x_k)_j] \times[x_l-(x_l)_j] \tag{30.3}$$

with limit values

$$\lim_{r\to 0}\hat{u}_{j,l}=0 \quad \lim_{r\to 0}\hat{u}_{j,ll}=\frac{c}{2} \quad \lim_{r\to 0}\hat{u}_{j,kl}=0. \tag{31}$$

4 Numerical implementation of the method

The method handles the formulated integral equations of the homogeneous solution using the standard BEM. The boundary is divided into N constant elements, and a set of M collocation points is selected within the domain (Fig. 2). Also, the time domain of interest $[0, T]$ is discretized into n small time intervals of size Δt.

To eliminate the boundary quantities $\bar{u}_i$, $\bar{u}_{i,n}$ from the equations of motion, the following matrix relation:

$$\begin{bmatrix}\mathbf{H}^b & \mathbf{G}^b\\ \mathbf{T}_i^b & \mathbf{S}_i^b\end{bmatrix}\begin{bmatrix}\bar{\mathbf{u}}_i\\ \bar{\mathbf{u}}_{i,n}\end{bmatrix}=\begin{bmatrix}\mathbf{0}\\ \tilde{\mathbf{d}}_i\end{bmatrix}+\begin{bmatrix}\mathbf{0}\\ \hat{\mathbf{U}}^b\end{bmatrix}\boldsymbol{\alpha}^{(i)} \tag{32}$$

is formulated at each material direction $x_i (i = 1, 2)$ from the discretized counterparts of BIE (21) and Eqs. (17), (18.1), when applied to each boundary node in turn. Here, $\bar{\mathbf{u}}_i$, $\bar{\mathbf{u}}_{i,n}$ are $N \times 1$ arrays including the nodal values of the boundary components of the homogeneous solution and its normal derivative, respectively;

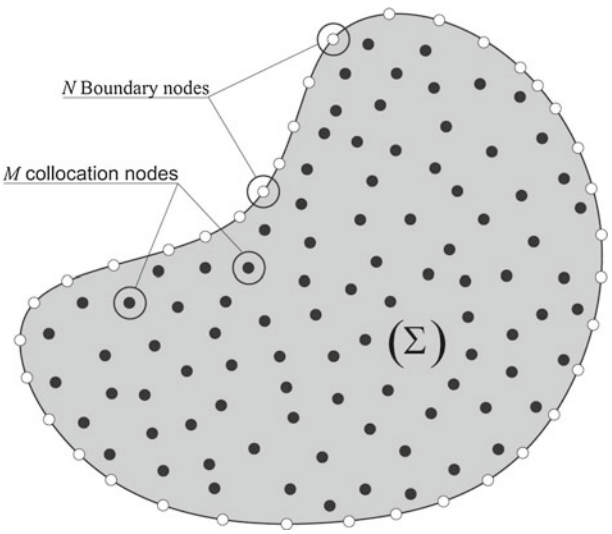

Fig. 2 Boundary discretization and distribution of collocation points

$\boldsymbol{\alpha}^{(i)}$ is an $M \times 1$ array composed from the values of the unknown time-dependent expansion coefficients at the collocation points inside Σ. $\mathbf{H}^b$ and $\mathbf{G}^b$ are $N \times N$ known coefficient matrices with elements resulting from the integration of $u^*_{,n}$ and u^* on the boundary elements; $\tilde{\mathbf{d}}_i$ is an $N \times 1$ array, which contains the prescribed boundary tractions and displacements; $\hat{\mathbf{U}}^b$ is an $N \times M$ matrix with elements $\hat{U}^b_{ij} = \hat{u}_j(\mathbf{x}_i, \mathbf{x}_j)$ at nodes where displacements are prescribed and elements $\hat{U}^b_{ij}$ resulting from the application of the differential operators $\mathcal{T}_{pq}$ on $\hat{u}_j$, at nodes where tractions are prescribed. The $N \times N$ matrices $\mathbf{T}^b_i$, $\mathbf{S}^b_i$ contain the coefficients of the unknown quantities from Eqs. (17) and (18.1), in which the derivatives $\bar{u}_{i,s}$ are approximated in terms of $\bar{u}_i$ using numerical differentiation.

Solving (32) for boundary values and substituting into the discretized counterpart of Eq. (20), given by

$$\mathbf{u}_i = \hat{\mathbf{U}}^d \boldsymbol{\alpha}^{(i)} + \left[\mathbf{H}^d \; -\mathbf{G}^d\right] \begin{bmatrix} \bar{\mathbf{u}}_i \\ \bar{\mathbf{u}}_{i,n} \end{bmatrix}, \tag{33}$$

the displacements at M collocation points are given by

$$\begin{aligned} \mathbf{u} = [\mathbf{u}_1 \quad \mathbf{u}_2]^T &= \begin{bmatrix} \mathbf{W}^{(1)} & \mathbf{0} \\ \mathbf{0} & \mathbf{W}^{(2)} \end{bmatrix} \boldsymbol{\alpha} + \begin{bmatrix} \mathbf{w}^{(1)} \\ \mathbf{w}^{(2)} \end{bmatrix} \\ &= \mathbf{W}\boldsymbol{\alpha} + \mathbf{w}, \end{aligned} \tag{34}$$

where $\mathbf{u}_i (i = 1, 2)$ are $M \times 1$ arrays, which contain the values of the i-component of displacement at the M domain collocation points; $\mathbf{H}^d$, $\mathbf{G}^d$ and $\hat{\mathbf{U}}^d$ are matrices evaluated as previously defined $\mathbf{H}^b$, $\mathbf{G}^b$ and $\hat{\mathbf{U}}^b$ except that in the former the source point takes values from the set $\{\mathbf{x}_j\}_{j=1}^M$ of the collocation points. $\mathbf{W}^{(i)}$ and $\mathbf{w}^{(i)}$ are M square matrices and arrays with elements resulting from the multiplication of known matrices.

Collocating Eqs. (25) results in

$$\mathbf{l}_{pq}(u_i) = \hat{\mathbf{U}}^d_{pq} \boldsymbol{\alpha}^{(i)} + \left[\mathbf{H}^d_{pq} \; -\mathbf{G}^d_{pq}\right] \begin{bmatrix} \bar{\mathbf{u}}_i \\ \bar{\mathbf{u}}_{i,n} \end{bmatrix}, \tag{35}$$

and after the elimination of boundary quantities using Eq. (32) we obtain the arrays $\mathbf{l}_{pq}(u_i)$, which contain the values of the differential operators $\mathcal{L}_{pq}(u_i)$ at the M collocation points, i.e.,

$$\mathbf{l}_{pq}(u_i) = \mathbf{W}^{(i)}_{pq} \boldsymbol{\alpha}^{(i)} + \mathbf{w}^{(i)}_{pq} \quad (p, q = 1, 2). \tag{36}$$

$\mathbf{H}^d_{pq}$, $\mathbf{G}^d_{pq}$ are $M \times N$ matrices with elements from the integration of $\mathcal{L}_{pq}(u^*_{,n})$ and $\mathcal{L}_{pq}(u^*)$ on the boundary elements, respectively; $\hat{\mathbf{U}}^d_{pq}$ is an M square matrix with elements $(U^d_{pq})_{ij} = \mathcal{L}_{pq}(\hat{u}_j)$. Moreover, $\mathbf{W}^{(i)}_{pq}$, $\mathbf{w}^{(i)}_{pq}$ are M square matrices and arrays with known elements, resulting from matrix operation among previously calculated matrices.

The final step of the proposed method is to collocate Eq. (7.1) at the M domain collocation points. The substitution of Eqs. (34) and (36) into the discretized equations of motion results in the following system of $2M$ equations:

$$\mathbf{W}^{(1)}_{11}\boldsymbol{\alpha}^{(1)} + \mathbf{W}^{(2)}_{12}\boldsymbol{\alpha}^{(2)} + \mathbf{w}^{(1)}_{11} + \mathbf{w}^{(2)}_{12} + \mathbf{b}_1 + \rho\mathbf{w}^{(1)}_t = \rho\mathbf{W}^{(1)}\ddot{\boldsymbol{\alpha}}^{(1)}, \tag{37.1}$$

$$\mathbf{W}^{(1)}_{21}\boldsymbol{\alpha}^{(1)} + \mathbf{W}^{(2)}_{22}\boldsymbol{\alpha}^{(2)} + \mathbf{w}^{(1)}_{21} + \mathbf{w}^{(2)}_{22} + \mathbf{b}_2 + \rho\mathbf{w}^{(2)}_t = \rho\mathbf{W}^{(2)}\ddot{\boldsymbol{\alpha}}^{(2)}, \tag{37.2}$$

in which $\mathbf{w}^{(i)}_t$ are arrays depending on the accelerations of prescribed displacements and the second time derivatives of prescribed tractions at the boundary. The system is solved using a time integration scheme based on the Houbolt method [21], which gave the best results with the smallest fluctuations. The applied time step Δt for the integration of the equations is calculated from

$$\Delta t = \min\left\{\beta \frac{d_{\min}}{c_{\max}}, 0.01 T_n\right\}, \tag{38}$$

in which β represents a nondimensional number with values greater or equal to 0.4716 [22], $d_{\min}$ is the minimum distance between the collocation points and the boundary points; $c_{\max}$ is the maximum value between the quasi longitudinal $c_L = (c_{22}/\rho)^{0.5}$ and the quasi transverse $c_T = (c_{66}/\rho)^{0.5}$ wave velocities; T_n is the fundamental period of the problem.

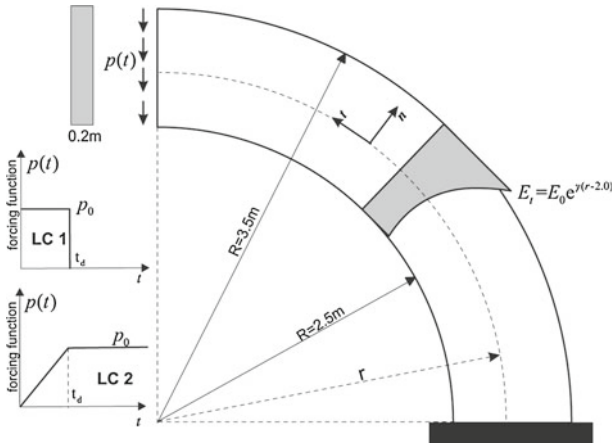

Fig. 3 Geometry and loading for the curved FGM cantilever beam

The interpolation coefficients at each discrete time $n\Delta t (n = 1, 2, \ldots)$ are obtained from the solution of Eq. (37.1). Subsequently, the coefficients $\{\alpha_j^{(i)}(t)\}_{j=1}^{M}$ are employed into Eq. (34) to evaluate the displacement components at the M collocation points. From the integral equations eliminated unknown boundary quantities can be found from the solution of Eq. (32) after the substitution of the calculated interpolation coefficients. Also, the stress components σ_{ij} are obtained at each collocation point from Eq. (4) using the discretized counterpart of (22) for the derivatives of the displacements. For any other point within the domain, not coincident with the selected $\{\mathbf{x}_j\}_{j=1}^{M}$, the components of the stress and strain fields can be computed from the discretized counterpart of the respective integral equation for the displacements and their spatial derivatives.

5 Numerical examples

To demonstrate the accuracy of the method, three example problems dealing with the transient dynamic analysis of nonhomogeneous, anisotropic plane elastic bodies were analyzed. Computationally, the results obtained by the method were checked with other numerical procedures (FEM) and found very close. In each example, the positions of the collocation points are selected in such a way that the nonhomogeneity and anisotropy of the material is best captured. Since the problem of obtaining accurate global interpolants using a multivariate approximation with MQs is strongly influenced by the selection of c [23,24], the calculation of an optimal value within an interval in which the constructed interpolants are cone-like functions [24–26] resolves the issue of selection using empirical formulae or numerical experiments. In this optimization procedure, the total potential energy of the system is used as the objective functional. The components of the displacement and their spatial derivatives are expressed within the functional in terms of the expansion coefficients and the shape parameter of the MQs. From the solution of this optimization problem, an optimal value for the shape parameter is calculated and used in the dynamic problem. The regular distribution schemes employed in the examples are selected from a sequence of increasingly refined grids until the results converge satisfactorily. Using these finer grids of collocation points, stable solutions are expected since small perturbations in the location of the points have little influence on the obtained results [27,28].

The presented formulation has been implemented into the BEM program TranNhAn, which uses the AEM with integral techniques, MQs as interpolation functions and the Houbolt method for the time integration of the resulting equations of motion.

5.1 Analysis of a curved FGM cantilever beam

We examine the response of a circular cantilever beam, under a uniformly distributed time-varying load along its tip, as depicted in Fig. 3. Numerical calculations are carried out for a functionally graded material in which the tangential modulus of elasticity varies according to the law $E_t = E_o e^{\gamma(r-2)}$, while E_r is constant and equal to E_o, everywhere. The numerical results are obtained for the following material properties: $E_o = 5{,}000$ Mpa,

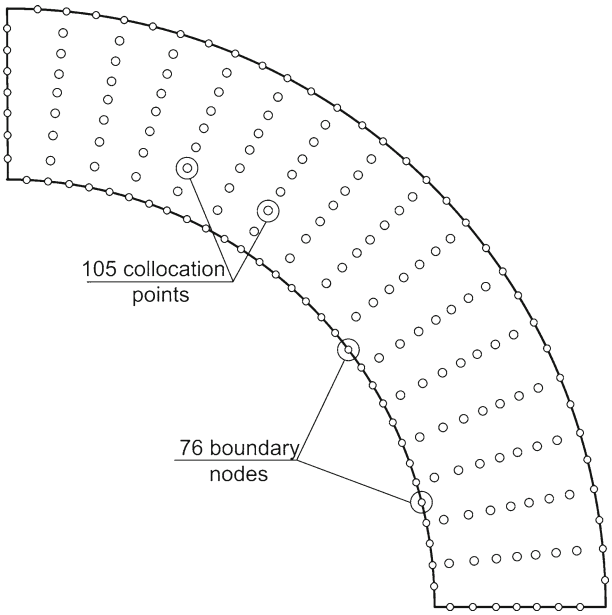

Fig. 4 Boundary discretization and pattern of collocation points

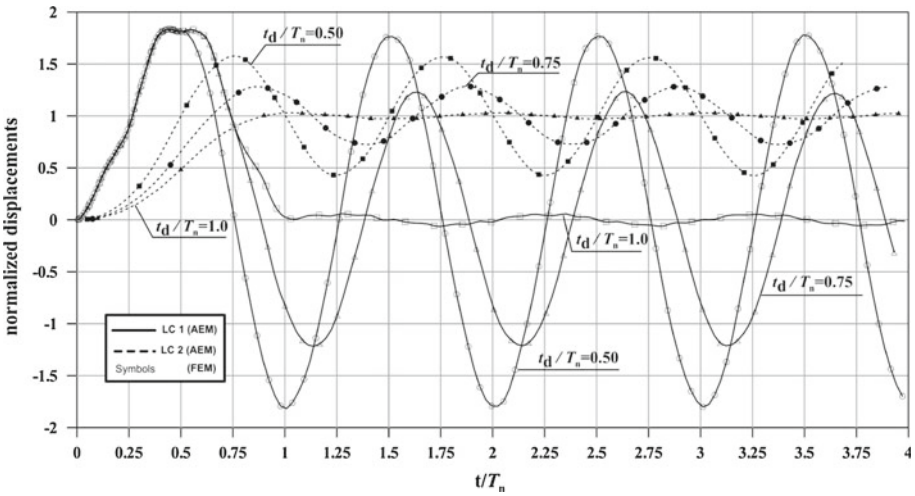

Fig. 5 Normalized displacements against normalized time for various rise times t_d of loading

$\nu = 0.3$, $G = 0.385E_t$ and material density $\rho = 10\,\text{Mg/m}^3$. We examine two load cases. In the first (LC1), the applied load is represented by a rectangular pulse of duration t_d with amplitude $p_o = 750\,\text{kN/m}^2$, and in the second (LC2) by a ramp function that has a finite rise time t_d while remaining constant thereafter at the value of $750\,\text{kN/m}^2$. The boundary is discretized into $N = 76$ boundary elements, whereas a pattern of $M = 105$ domain points is chosen having a denser distribution along the radial direction where the material gradients are large, as schematically presented in Fig. 4. Several plots of normalized displacement, $\max u_2(t)/\max u_2^{st}$, against normalized time, t/T_n, with u_2^{st} the maximum static deflection and T_n the fundamental period of the beam, are presented in Fig. 5 and compared with the results obtained from the FEM package ANSYS using a mesh of 685 quadratic finite elements. Moreover, in Fig. 6 the displacements and in Fig. 7 the tangential stresses for LC1 and LC2 are plotted along the perimeter of the beam (counterclockwise from point A) for different values of the graded parameter, at times where the maximum displacements occur.

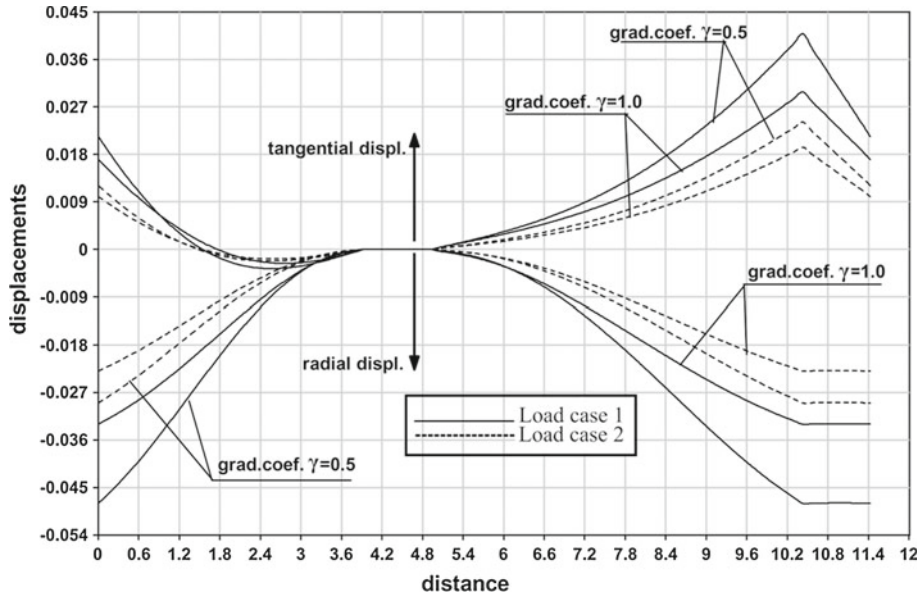

Fig. 6 Distribution of radial and tangential displacement along the boundary of the beam

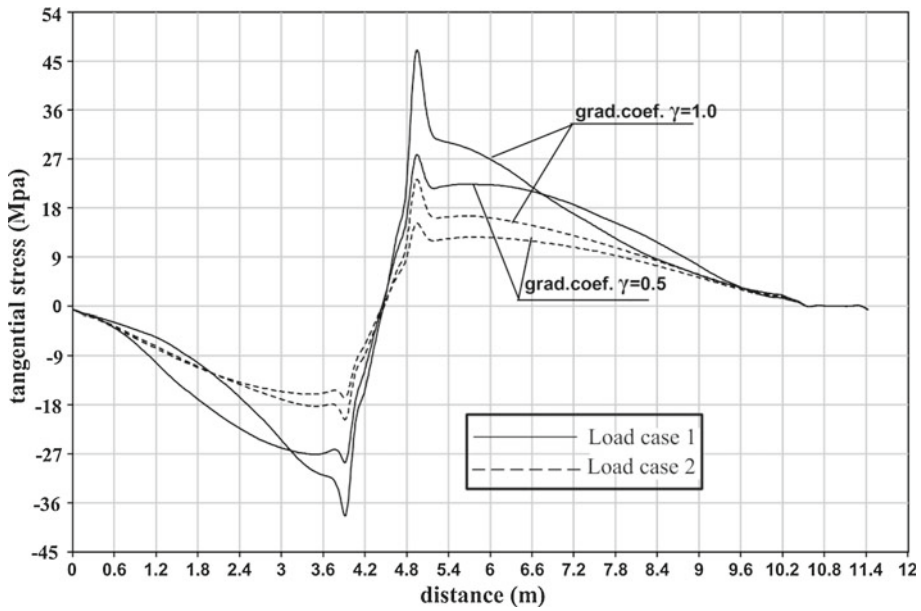

Fig. 7 Distribution of tangential stress along the boundary of the beam

5.2 Circular disc with a concentric hole

Consider the unit width circular disc of radius R with a concentric hole of radius r shown in Fig. 8. The disc is subjected to a time-varying sinusoidal pressure $\tilde{t}_r(t)$ and shear tractions $\tilde{t}_t(t)$, with amplitude 50 kN/m^2 and circular frequencies Ω and 0.5Ω, respectively. The time duration of the loading is $t_d = 0.3$ s. Due to symmetry, only one-quarter of the disc is modeled. Numerical calculations are carried out for a functionally graded material with an exponential variation in the radial modulus of elasticity, according to the law $E_r = E_o e^{\gamma(r-1)}$, while E_t is constant and equal to E_o everywhere. The employed data are as follows: $R = 2.5$ m, $r = 1.0$ m, $E_o = 1{,}000$ Mpa, $\nu = 0.3$, $G = 0.385E_t$, $\rho = 10$ Mg/m^3.

The problem was analyzed using $N = 90$ constant boundary elements and $M = 88$ interior collocation points, as shown in Fig. 9. To compare the obtained results, the FEM code ANSYS was employed using 585

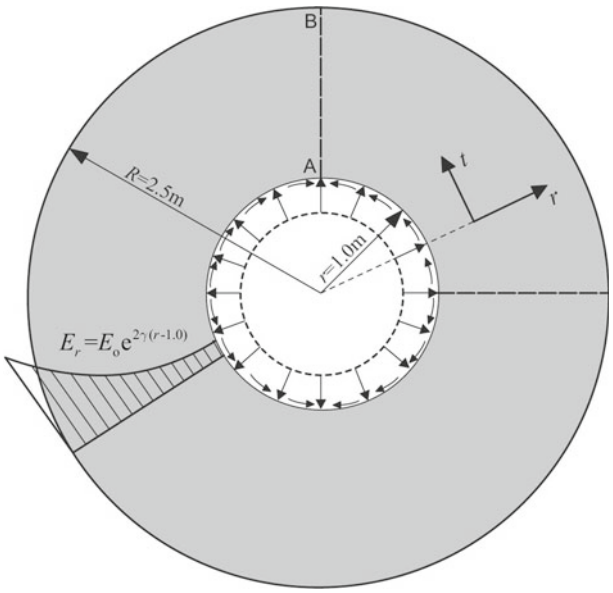

Fig. 8 Circular disc with a concentric hole

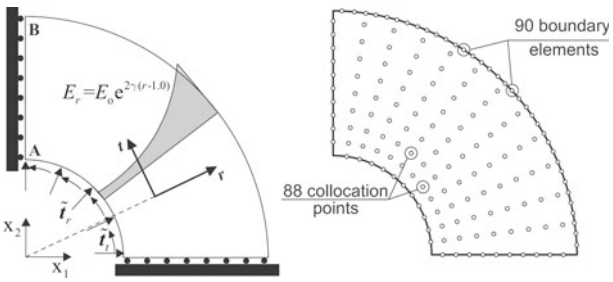

Fig. 9 One-quarter modeling of the disc. Boundary nodes and domain collocation pattern

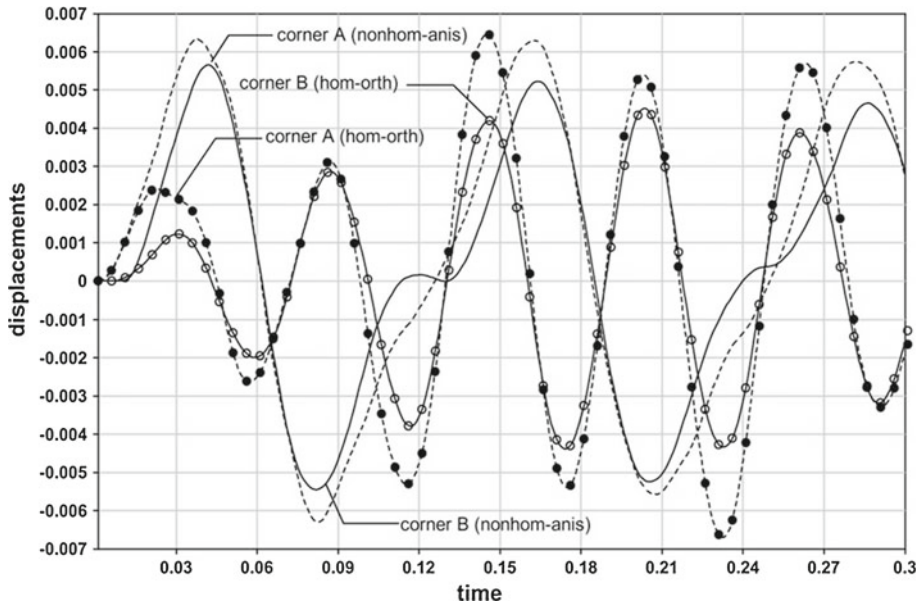

Fig. 10 Time history of radial displacement at points A and B

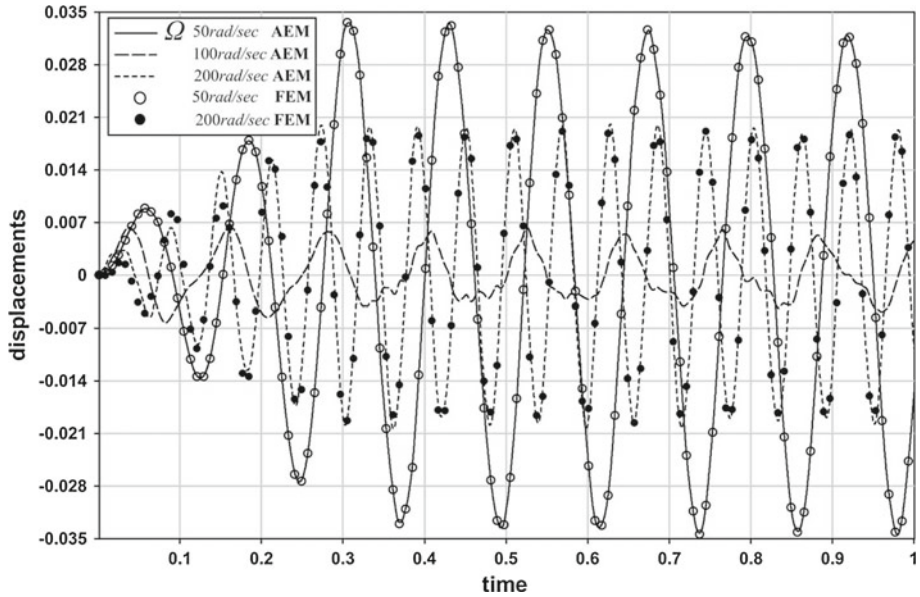

Fig. 11 Time history of radial displacement at point A for various forcing frequencies Ω

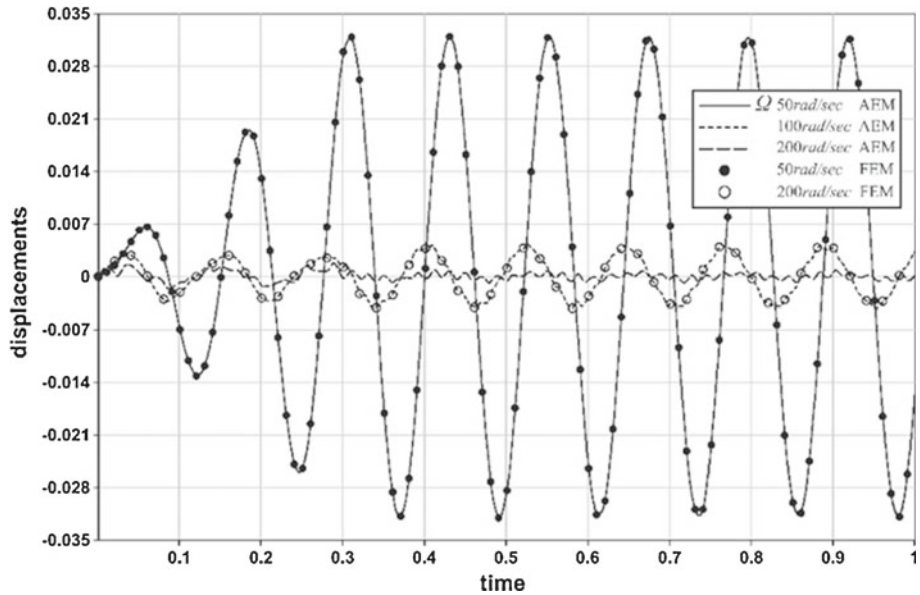

Fig. 12 Time history of tangential displacement at point A for various values of forcing frequency Ω

four-node isoparametric elements. The time history of radial displacement at points A and B is presented in Fig. 10, for $\gamma = 1$, $\Omega = 100$ rad/s, and compared with the response obtained for homogeneous orthotropic material having $E_r = E_o$ and E_t the mean value of the tangential modulus in the nonhomogeneous case.

Moreover, in Figs. 11 and 12, the time history of radial and tangential displacement at point A is compared with the results calculated from the FEM solution for different values of the forcing frequency Ω. The distribution of radial and tangential displacements along the perimeter of the disc (counterclockwise from A) at $t = 65$ msec, for $\Omega = 100$ rad/s, is plotted in Fig. 13, for different values of the graded parameter γ. For the same Ω, the distribution of tangential stress along the perimeter of the disc is plotted in Fig. 14, for different values of γ.

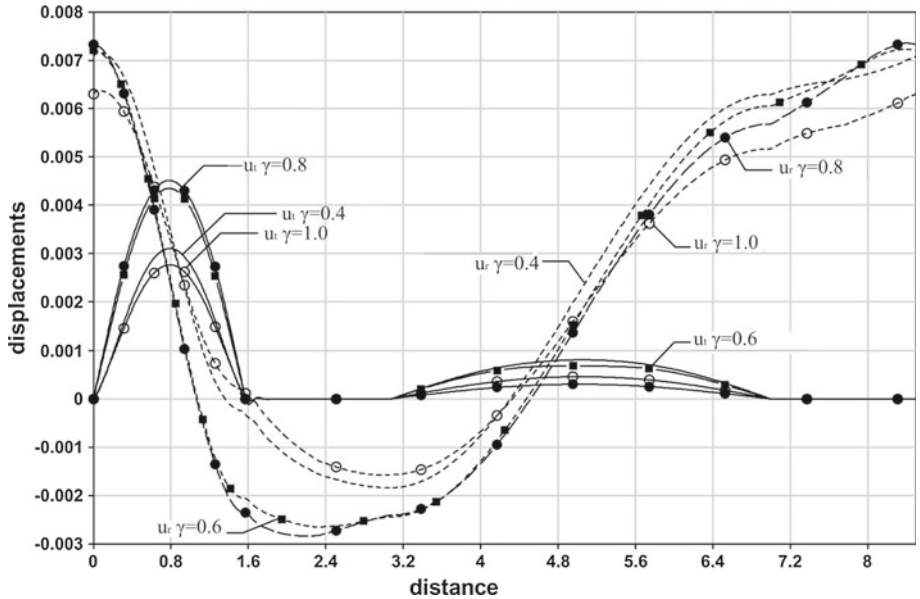

Fig. 13 Distribution of radial and tangential displacement along the boundary at $t = 65$ msec for $\Omega = 100$ rad/s

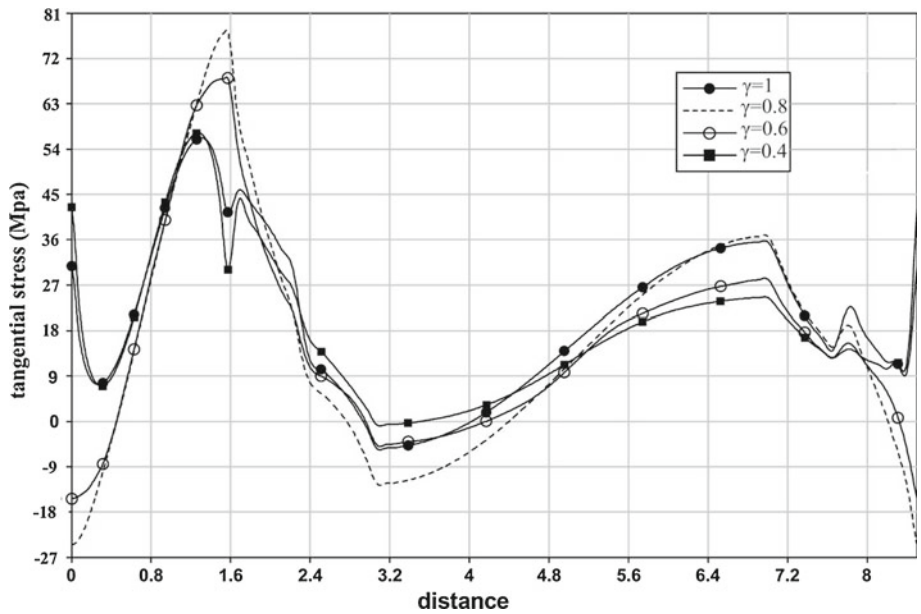

Fig. 14 Distribution of tangential stress along the boundary for $\Omega = 100$ rad/s at $t = 65$ msec

5.3 Homogeneous orthotropic disc with semi-circular cuts

We examine the homogeneous orthotropic disc with semi-circular edge cuts, depicted in Fig. 15. The disc is subjected to uniform tensile tractions $\tilde{t}_1(x, t)$ on the vertical straight parts of the boundary, which can be represented by a time function resulting from the addition of three sinusoidals of the same amplitude and circular frequencies Ω_1, Ω_2 and Ω_3, respectively. The duration of the input is set to: $t_d = 2$ s. Due to the symmetry of the problem, only one-quarter of the disc is modeled. The employed data of the material are as follows: $E_1 = 1{,}000$ Mpa, $G = 1{,}000$ Mpa, $\nu = 0.2$, $\rho = 10$ Mg/m^3 and $E_2 = \alpha E_1$, with α the anisotropy coefficient which takes values between 1 and 10. We examine two load cases. Load case 1 (LC1) is constructed with $\Omega_1 = 25$ rad/s, $\Omega_2 = 50$ rad/s and $\Omega_3 = 75$ rad/s, whereas load case 2 (LC2) with $\Omega_1 = 100$ rad/s, $\Omega_2 = 125$ rad/s and $\Omega_3 = 150$ rad/s. The amplitude on both cases is set to: $\tilde{t}_o(\mathbf{x}) = 1$ Mpa. The problem was analyzed using $N = 63$ constant boundary elements and $M = 135$ interior collocation

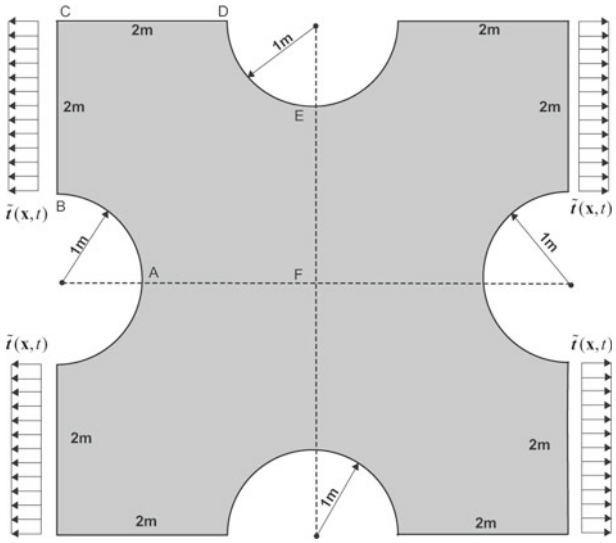

Fig. 15 Homogeneous orthotropic disc with semi-circular cuts

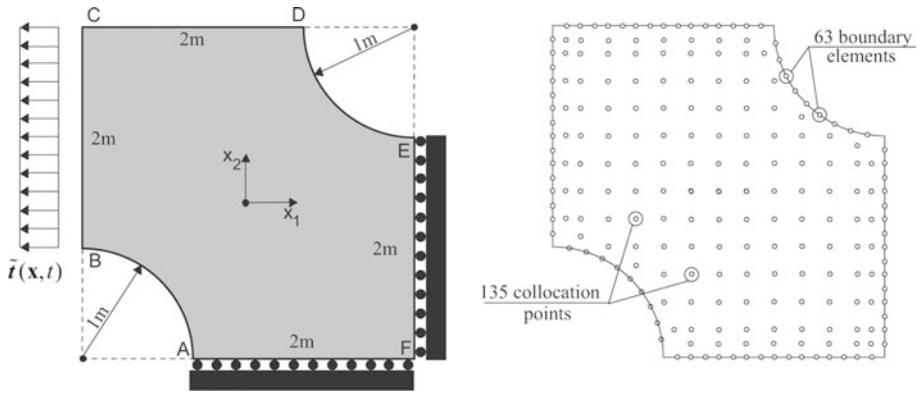

Fig. 16 One-quarter modeling of the disc. Boundary discretization and domain collocation pattern

points, as shown in Fig. 16. In Figs. 17 and 18, the maximum disc displacements are plotted against α for both load cases and compared with those obtained from the FEM package ANSYS using 1325 four-node isoparametric elements. Moreover, the time history of the horizontal displacement at point C is plotted for LC1, for two values of the anisotropy coefficient, as shown in Fig. 19. Also, in Fig. 20, the time history of the maximum horizontal displacement is plotted with $\alpha = 1.9$, for LC2.

6 Conclusions

In this paper, the transient dynamic analysis of nonhomogeneous, anisotropic, plane elastic bodies is examined by a boundary-only method based on the concept of the analog equation. From the presented analysis and the solution of the selected numerical examples, the following main conclusions can be drawn.

- The method, as a boundary-only method, has all the advantages of the BEM, i.e., the discretization and integration are performed on the boundary only. Comparing to other boundary-only methods and specifically the dual reciprocity method (DRM), we can conclude that the presented method is alleviated from the restrictions and drawbacks characterizing the DRM. Thus, the fundamental solution to Laplace's equation is employed to derive the integral representation of the solution in contrast to the DRM, where the extraction of a standard linear differential operator from the governing equations of the problem is not always possible, or the fundamental solution of the adjoint operator cannot be established.

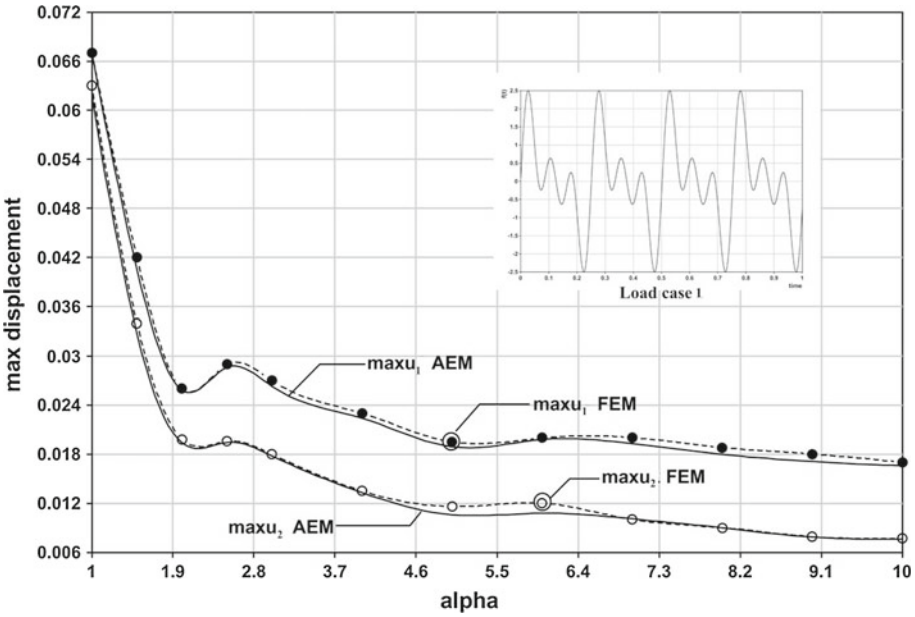

Fig. 17 Dependence of maximum developed displacement from anisotropy coefficient (LC1)

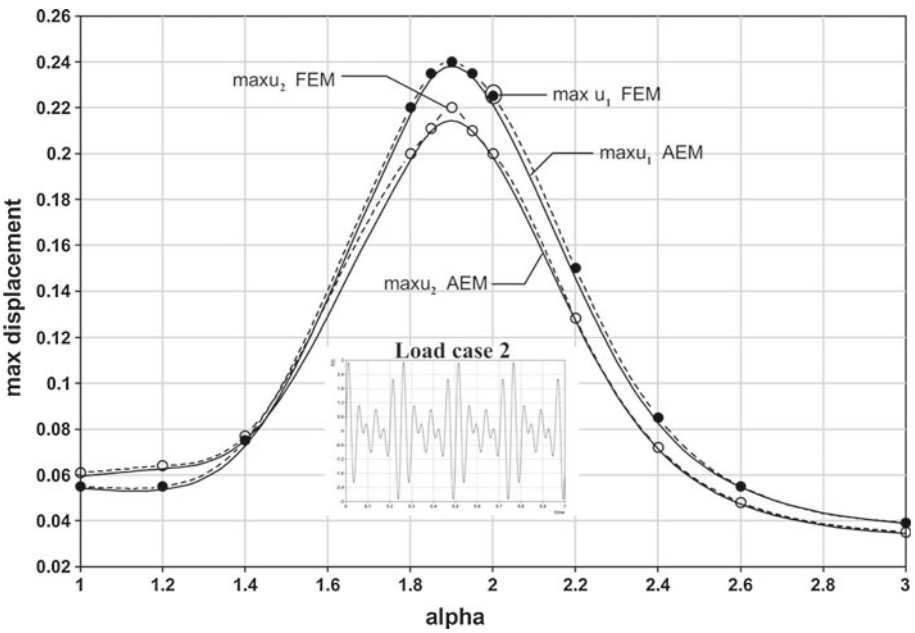

Fig. 18 Dependence of maximum developed displacement from anisotropy coefficient (LC2)

- The proposed method is considered as an alternative to domain discretization methods, such as the FEM, with its major advantage being that the discretized equations of motion are formed without the use of a predefined mesh. The set of interior nodes, which are uniformly scattered within the body following the geometry and the nonhomogeneity of the system in a simple geometric pattern, are used to represent and not to discretize the domain. Since they do not form a mesh, no information on the relationship between the nodes is required. Thus, a considerable time is saved in modeling projects, and flexibility is provided in adding, deleting or relocating a node whenever needed.

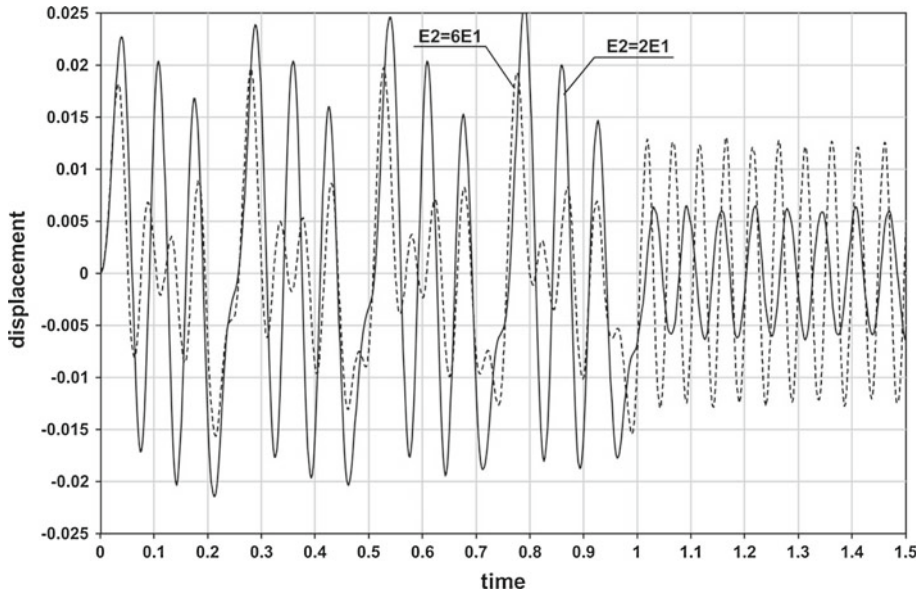

Fig. 19 Time history of horizontal displacement at point C (LC1)

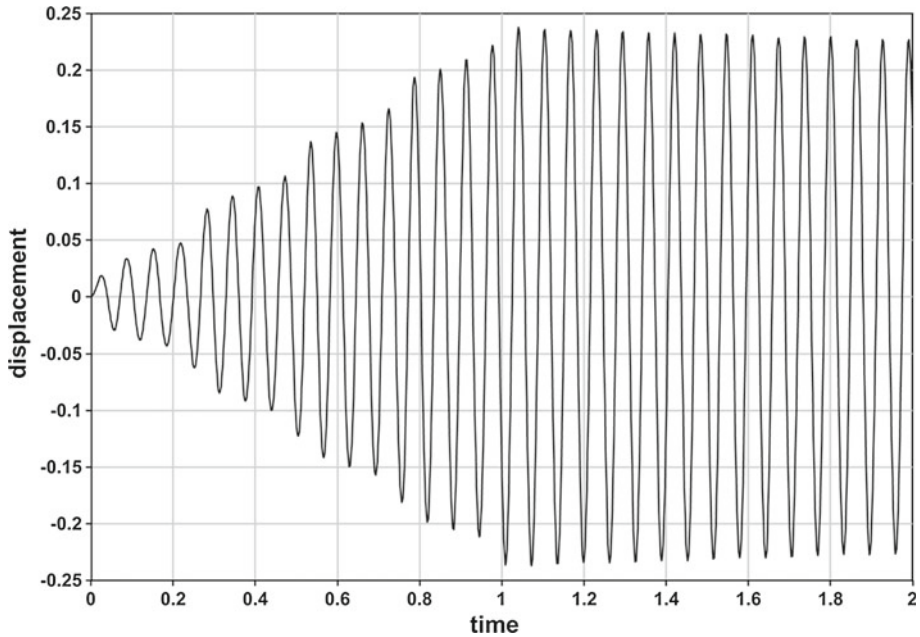

Fig. 20 Time history of horizontal displacement at point C (LC2)

- The displacements and the stress components can be computed at any position within the domain and on the boundary using the respective integral representation of the quantity as mathematical formulas.

References

1. Beskos, D.E.: Boundary element methods in dynamic analysis, Part II, 1986–1996. Appl. Mech. Rev. **50**, 149–197 (1997)
2. Manolis, G.D., Shaw, R.P.: Fundamental solutions for variable density 2-D elastodynamic problems. Eng. Anal. Bound. Elem. **24**, 739–750 (2000)
3. Rangelov, T.V., Manolis, G.D., Dineva, P.S.: Elastodynamic fundamental solutions for certain families of 2-D inhomogeneous anisotropic domains: basic derivations. Eur. J. Mech. A Solids **24**, 820–836 (2005)

4. Wang, C.Y., Achenbach, G.D.: Two dimensional time domain BEM for scattering of elastic waves in solids of general anisotropy. Int. J. Solids Struct. **33**, 3843–3864 (1996)
5. Zhang, C.: Transient elastodynamic antiplane crack analysis of anisotropic solids. Int. J. Solids Struct. **37**, 6107–6130 (2000)
6. Cruse, T.A, Swedlow, J.L.: Interactive program for analysis and design problems in advanced composites. Technical report, Carnegie-Mellon University. Report AFLM-TR-71-268 (1971)
7. Albuquerque, E.L., Sollero, P., Aliabadi, M.H.: The boundary element method applied to time dependent problems in anisotropic materials. Int. J. Solids Struct. **39**, 1405–1422 (2002)
8. Albuquerque, E.L., Sollero, P., Fedelinski, P.H.: Free vibration analysis of anisotropic materials structures using the boundary element method applied to time dependent problems in anisotropic materials. Eng. Anal. Bound. Elem. **27**, 977–985 (2003)
9. Atluri, S.N., Sladek, J., Sladek, V., Zhu, T.: The local boundary integral equation (LBIE) and its meshless implementation for linear elasticity. Comput. Mech. **25**, 180–198 (2000)
10. Sladek, J., Sladek, V., Atluri, S.N.: Local boundary integral equation (LBIE) method for solving problems of elasticity with nonhomogeneous material properties. Comput. Mech. **24**, 456–462 (2000)
11. Sladek, V., Sladek, J., Zhang, C.: Local integro-differential equations with domain elements for numerical solution of PDE with variable coefficients. J. Eng. Math. **51**, 261–282 (2005)
12. Sladek, J., Sladek, V., Zhang, C.: Application of meshless local Petrov-Galerkin (MLPG) method to elastodynamic problems in continuously nonhomogeneous solids. Comput. Model. Eng. Sci. **4**, 637–648 (2000)
13. Sladek, J., Sladek, V., Atluri, S.N.: Meshless Local Petrov-Galerkin in anisotropic elasticity. Comput. Model. Eng. Sci. **5**, 477–489 (2003)
14. Sladek, V., Sladek, J., Tanaka, M., Zhang, C.: Local integral equation method for potential problems in functionally graded anisotropic materials. Eng. Anal. Bound. Elem. **29**, 829–843 (2005)
15. Katsikadelis, J.T.: The analog boundary integral equation method for nonlinear static and dynamic problems in continuum mechanics. J. Theor. Appl. Mech. **40**, 961–984 (2002)
16. Katsikadelis, J.T.: The BEM for nonhomogeneous bodies. Arch. Appl. Mech. **74**, 780–789 (2005)
17. Nerantzaki, M.S., Kandilas, C.B.: Geometrically nonlinear analysis of elastic membranes with embedded inclusions. Eng. Anal. Bound. Elem. **31**, 216–225 (2007)
18. Kandilas, C.B., Nerantzaki, M.S.: Nonlinear transient dynamic response of elastic membranes with embedded inclusions. Eng. Anal. Bound. Elem. **32**, 824–838 (2008)
19. Nerantzaki, M.S., Kandilas, C.B.: A boundary element method solution for anisotropic nonhomogeneous elasticity. Acta Mech. **200**, 199–211 (2008)
20. Buhmann, M.D.: Radial Basis Functions: Theory and Implementations. Cambridge Monographs on Applied and Computational Mathematics. Cambridge University Press, Cambridge (2004)
21. Hughes, T.J.R., Liu, W.K.: Implicit-explicit finite elements in transient analysis: stability theory. ASME J. Appl. Mech. **45**, 371–374 (1978)
22. Albuquerque, E.L., Sollero, P., Aliabadi, M.H.: The boundary element method applied to time dependent problems in anisotropic materials. Int. J. Solids Struct. **39**, 1405–1422 (2002)
23. Kansa, E.J., Hon, Y.C.: Circumventing the ill-conditioning problem with multiquadrics radial basis functions: applications to elliptic differential equations. Comput. Math. Appl. **39**, 123–137 (2000)
24. Kansa, E.J.: Multiquadrics—a scattered data approximation scheme with applications to computational fluid-dynamics-I. Comput. Math. Appl. **8**, 127–145 (1990)
25. Goldberg, M.A., Chen, C.S., Kapur, S.P.: Improved multiquadrics approximation for partial differential equations. Eng. Anal. Bound. Elem. **18**, 89–95 (1996)
26. Hardy, R.L.: Multiquadric equations of topography and other irregular surfaces. J. Geophys. Res. **176**, 1905–1915 (1971)
27. Katsikadelis, J.T.: The meshless analog equation method: I. Solution of elliptic partial differential equations. Arch. Appl. Mech. **79**, 557–578 (2009)
28. Katsikadelis, J.T.: A generalized Ritz method for partial differential equations in domains of arbitrary geometry using global shape functions. Eng. Anal. Bound. Elem. **32**, 353–367 (2008)